J. Fluid Mech. (1967), *vol.* 29, *part* 1, *pp.* 39–60
Printed in Great Britain

Detached shear layers in a rotating fluid

By R. HIDE

Department of Geology and Geophysics, and Department of Physics, Massachusetts Institute of Technology, Cambridge, Massachusetts

AND C. W. TITMAN

School of Physics, University of Newcastle upon Tyne, Newcastle upon Tyne 1

(Received 22 August 1966)

The occurrence of detached shear layers should, according to straightforward theoretical arguments, often characterize hydrodynamical motions in a rapidly rotating fluid. Such layers have been produced and studied in a very simple system, namely a homogeneous liquid of kinematical viscosity ν filling an upright, rigid, cylindrical container mounted coaxially on a turn-table rotating at Ω_0 rad/s about a vertical axis, and stirred by rotating about the same axis at Ω_1 rad/s a disk of radius a cm and thickness b' cm immersed in the liquid with its plane faces parallel to the top and bottom end walls of the container. By varying Ω_0, Ω_1 and a, ranges of Rossby number, the modulus of $\epsilon \equiv (\Omega_1 - \Omega_0)/\frac{1}{2}(\Omega_1 + \Omega_0)$, from 0·01 to 0·3, and Ekman number, $E \equiv 2\nu/a^2(\Omega_1 + \Omega_0)$, from 10^{-5} to 5×10^{-4} were attained. Although the apparatus was axisymmetric, only when $|\epsilon|$ did not exceed a certain critical value, $|\epsilon_T|$, was the flow characterized by the same property of symmetry about the axis of rotation. Otherwise, when $|\epsilon| > |\epsilon_T|$, non-axisymmetric flow occurred, having the form in planes perpendicular to the axis of rotation of a regular pattern of waves, M in number, when ϵ was positive, and of a blunt ellipse when ϵ was negative.

The axial flow in the axisymmetric detached shear layer, and the uniform rate of drift of the wave pattern characterizing the non-axisymmetric flow when ϵ is positive, depend in relatively simple ways on ϵ and E. The dependence of $|\epsilon_T|$ on E can be expressed by the empirical relationship $|\epsilon_T| = AE^n$, where $A = 16{\cdot}8 \pm 2{\cdot}2$ and $n = 0{\cdot}568 \pm 0{\cdot}013$ ($= (4/7) \times (1{\cdot}000 - (0{\cdot}005 \pm 0{\cdot}023))$!), standard errors, 25 determinations. M does not depend strongly on E but generally decreases with increasing ϵ.

1. Introduction

This paper reports an experimental study of detached shear layers produced in a rapidly rotating fluid under very simple conditions. The apparatus used is illustrated schematically in figure 1. It consisted of a cylindrical tank of internal radius R' and internal length D', within which was mounted coaxially a rigid disk of radius a and thickness b', the lower face of the disk being a distance d' above the bottom of the tank. Hydrodynamical motions in the homogeneous liquid of kinematical viscosity ν that completely filled the tank were generated by rotating the disk and the tank at different but constant angular speeds, Ω_1 and Ω_0 respectively, about their common axis of symmetry.

Straightforward theoretical considerations show that when a Rossby number, $|\epsilon|$, and an Ekman number, E, are sufficiently small to satisfy the conditions

$$|\epsilon| \ll 1 \quad \text{and} \quad E \ll \min[1, d^2, b^2, (D-b-d)^2], \tag{1.1a,b}$$

where

$$\epsilon \equiv 2(\Omega_1 - \Omega_0)/(\Omega_1 + \Omega_0), \tag{1.2}$$

$$E \equiv 2\nu/a^2(\Omega_1 + \Omega_0) \tag{1.3}$$

and

$$d \equiv d'/a, \quad D \equiv D'/a, \quad b = b'/a, \quad R = R'/a, \tag{1.4a–d}$$

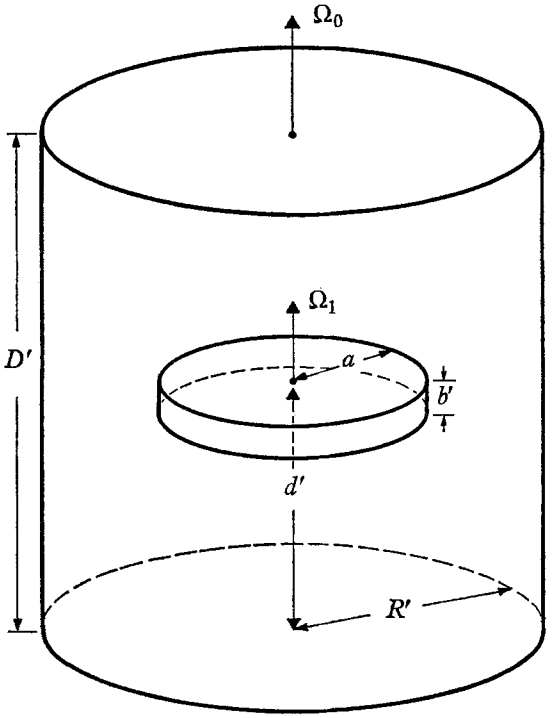

FIGURE 1. Schematic diagram of the apparatus (cf. figure 3).

regions of high shear may arise not only in regions k and l (see figure 2), the Ekman boundary layers on the flat surfaces of the disk (in $z' = 0$ and $z' = b'$) and over parts of the walls of the tank (in $z' = -d'$ and $z' = (D'-d')$), but also in region m, the vicinity of the cylindrical surface $r' = a$, where r' and z' are the radial and axial polar co-ordinates of a general point in a frame of reference whose origin is the point where the axis of rotation intersects the bottom of the disk. This prediction has been verified experimentally for negative as well as positive values of ϵ, over a range of conditions, obtained by varying Ω_1, Ω_0 and a, corresponding to $0{\cdot}01 < |\epsilon| < 0{\cdot}3$, $10^{-5} < E < 5 \times 10^{-4}$, $2{\cdot}94 < d < 8{\cdot}85$, $4{\cdot}05 < D < 12{\cdot}2$, $0{\cdot}067 < b < 0{\cdot}20$, $2{\cdot}54 < R < 7{\cdot}62$ (see table 1).

The experiments also show that, over the range of conditions studied, axisymmetric flow arises when $|\epsilon|$ does not exceed a certain critical value $|\epsilon_T|$ (say), where $|\epsilon_T|$ satisfies the empirical relationship

$$|\epsilon_T| = AE^n, \tag{1.5a}$$

where

$$A = 16{\cdot}8 \pm 2{\cdot}2 \quad \text{and} \quad n = 0{\cdot}568 \pm 0{\cdot}013, \tag{1.5b}$$

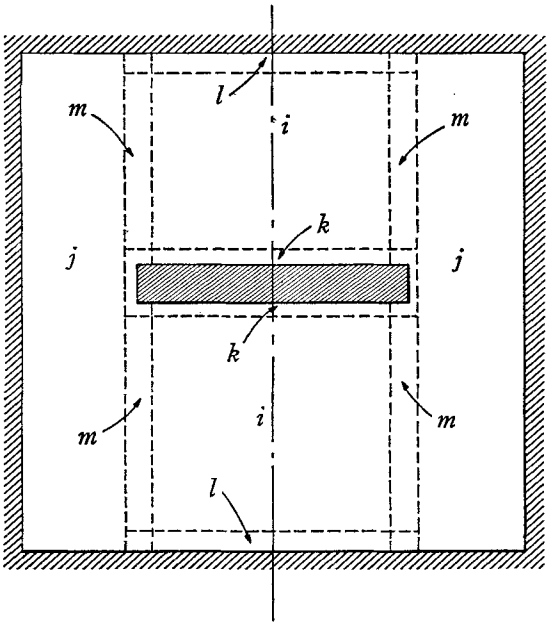

FIGURE 2. Illustration of the separation of the fluid into regions characterized by different balances of forces. As $|\epsilon|$ and E are very small, regions i and j are geostrophic, i.e. they are characterized by a balance between pressure forces and Coriolis forces. Region j rotates with the container at Ω_0 rad/s and regions i rotate at $\frac{1}{2}(\Omega_1+\Omega_0)$ rad/s. Hence, across the ageostrophic detached shear layer, region m, the angular speed of rotation changes by $\frac{1}{2}(\Omega_1-\Omega_0)$ rad/s. Regions k and l are Ekman boundary layers, which are ageostrophic and across which the angular speed of rotation changes from $\frac{1}{2}(\Omega_1+\Omega_0)$ rad/s, its value in regions i, to Ω_1 rad/s in the case of regions k and to Ω_0 rad/s in the case of regions l. Fluid particles within regions i move towards the disk at $(\Omega_1-\Omega_0)(2\nu/(\Omega_1+\Omega_0))^{\frac{1}{2}}$ cm/s, are accelerated radially outwards or inwards in regions k according as $\Omega_1 \gtrless \Omega_0$ and vice versa for regions l, and complete the meridional circuit via the detached shear layer, region m.

Parameter	Value	Parameter	Value
D' (cm)	30·0	ϵ	0·01–0·3
d' (cm)	22·0	E	10^{-5} to 5×10^{-4}
R' (cm)	19·0	d	2·94–8·85
b' (cm)	1·25	D	4·05–12·2
a (cm)	2·5–7·5	b	0·067–0·20
Ω_0 (rad/s)	1–14	R	2·54–7·62
$\Omega_1-\Omega_0$ (rad/s)	−1·5–3		
ν (cm^2 s^{-1})	0·010		

TABLE 1. Ranges of parameters covered by all the experiments

standard errors, 25 readings. When, however, $|\epsilon| > |\epsilon_T|$, the flow in region m (see figure 2) exhibits azimuthal variations which penetrate into regions i and j.

When ϵ is positive (i.e. $\Omega_1 > \Omega_0$) these azimuthal variations form a pattern of waves, M in number, in planes perpendicular to the z direction, where M generally decreases as ϵ increases, but does not depend strongly on E. Under most conditions, apart from drifting uniformly about the axis of rotation of the appa-

ratus at a rate, Ω_w rad/s, intermediate between Ω_1 and Ω_0, the fully developed wave-motion is quite steady. However, there are conditions, not yet fully investigated, under which the wave pattern may undergo regular repeating fluctuations reminiscent of one of the 'vacillation' phenomena discovered some time ago in certain thermal convection experiments (Hide 1953).

When ϵ is negative (i.e. $\Omega_1 < \Omega_0$), although the axisymmetric flow gives way to non-axisymmetric flow at about the same value of $|\epsilon_T|$ as in the case of positive ϵ, the pattern of azimuthal variations associated with the non-axisymmetric flow is then markedly different (see figures 4 and 5 below).

This paper is made up as follows: §2 contains a scale analysis of the hydrodynamical equations and a discussion, based on the Proudman–Taylor theorem and on the theory of a divergent Ekman layer, of the axisymmetric régime of flow; §3 deals with the design and construction of the apparatus, and with experimental techniques; §§4 and 5 describe, respectively, the general properties of the axisymmetric and non-axisymmetric régimes of flow and an investigation of the transition between these régimes (see equation (1.5) above); §6 describes an investigation of the dependence on z' (see figure 1) of a quantity $\hat{w}_m$, the extreme value of the z' component of flow in the detached shear layer. The results of this investigation can be summarized fairly well by the empirical relationship

$$\hat{w}'_m = \tilde{w}'_m/[1+z'/Z'_m], \tag{1.6}$$

where $\tilde{w}'_m$ and Z'_m depend on E and ϵ. §7 describes an investigation of the dependence on ϵ and E of certain properties (Ω_w and M) of the non-axisymmetric flow régime. Concluding remarks are made in §8 and some of the experimental results that are only summarized in the main part of the paper are given in greater detail in an appendix.

2. Theoretical considerations

Denote by $\mathbf{u}' = (u', v', w')$ the flow velocity at time t' at a point having cylindrical polar co-ordinates (r', ϕ', z') in a frame of reference which rotates uniformly with angular velocity $\Omega\mathbf{k}$ relative to a fixed frame, where $\mathbf{k}$ is a unit vector along the z'-axis and

$$\Omega \equiv \tfrac{1}{2}(\Omega_1 + \Omega_0), \tag{2.1}$$

the mean of the angular speeds of rotation of the disk and of the tank. Denote by ρ and ν respectively the density and kinematic viscosity of the fluid, and treat these quantities as uniform (i.e. independent of (r', ϕ', z', t')). Denote by P' the dynamic pressure divided by ρ.

Introduce the dimensionless quantities $\mathbf{u}$, u, v, w, r, ϕ, z, t, P defined by the following equations:

$$\mathbf{u}' \equiv U\mathbf{u}, \quad (u', v', w') \equiv U(u, v, w), \tag{2.2}$$

where

$$U \equiv a|\Omega_1 - \Omega_0| = a\Omega|\epsilon| \tag{2.3}$$

(see (1.2) and (2.1)),

$$r' \equiv ar, \quad \phi' \equiv \phi, \quad z' \equiv d'z, \quad t' \equiv ta/U \tag{2.4a–d}$$

and

$$P' \equiv \Omega U a P. \tag{2.5}$$

The Navier–Stokes equations of hydrodynamical motion and the equation of continuity of an incompressible fluid take the form:

$$-2v+P_r = -|\epsilon|\{u_t+uu_r+r^{-1}vu_\phi+d^{-1}wu_z-r^{-1}v^2\} + E[u_{rr}+r^{-1}u_r+r^{-2}u_{\phi\phi}+d^{-2}u_{zz}-r^{-2}u-2r^{-2}v_\phi], \quad (2.6)$$

$$2u+r^{-1}P_\phi = -|\epsilon|\{v_t+uv_r+r^{-1}vv_\phi+d^{-1}wv_z+r^{-1}uv\} + E[v_{rr}+r^{-1}v_r+r^{-2}v_{\phi\phi}+d^{-2}v_{zz}-r^{-2}v+2r^{-2}u_\phi], \quad (2.7)$$

$$d^{-1}P_z = -|\epsilon|\{w_t+uw_r+r^{-1}vw_\phi+d^{-1}ww_z\} + E[w_{rr}+r^{-1}w_r+r^{-2}w_{\phi\phi}+d^{-2}w_{zz}], \quad (2.8)$$

and

$$u_r+r^{-1}u+r^{-1}v_\phi+d^{-1}w_z = 0. \quad (2.9)$$

It follows immediately from (2.6)–(2.9) that when the right-hand sides of the first three of these equations vanish,

$$P_z = u_z = v_z = w_z = 0. \quad (2.10)$$

This is the celebrated Proudman–Taylor theorem (Proudman 1916; Taylor 1923), which should hold throughout most of the fluid to a degree of accuracy measured by $|\epsilon|$ and E when these parameters are very small.

The external parameter $|\epsilon|$ is, according to its definition (see (1.2) and (2.1)) and the scaling procedure implicit in (2.6) to (2.9), a measure of the average order of magnitude of the non-linear term $(\mathbf{u}'.\nabla')\mathbf{u}'$ in the dimensional equation of motion in terms of the magnitude of the Coriolis term $2\Omega\mathbf{k}\times\mathbf{u}'$ in the same equation. E, see (1.3) and (2.1), is the external dimensionless parameter involving the coefficient of kinematical viscosity ν; E measures the average order of magnitude of the viscous term, $\nu\nabla'^2\mathbf{u}'$, in the dimensional equation of motion in terms of the Coriolis term $2\Omega\mathbf{k}\times\mathbf{u}'$. By convention, $|\epsilon|$ is thus a Rossby number and E an Ekman number.

It is often convenient to think of the Rossby number as the magnitude of the vorticity of the relative motion divided by 2Ω, the vorticity of the basic rotation, and of the square root of the Ekman number as a ratio of the thickness, $(\nu/\Omega)^{\frac{1}{2}}$, of the thinnest parts of the viscous boundary layers present (see 2.17) to a characteristic linear dimension of the apparatus. Thus, the criteria expressed by (1.1) are equivalent to the requirements that the vorticity of relative motion be much less than that of the basic rotation, and that the apparatus be large enough for effectively inviscid regions to be present in the fluid, even though boundary layers and detached shear layers, in which viscous forces are not negligible, may also occur. Satisfaction of these criteria is the essential requirement for quasi-geostrophic motion, characterized by an approximate balance between pressure forces and Coriolis forces, to occur somewhere in the system.

When the flow is steady (i.e. $\partial\mathbf{u}/\partial t = 0$) and axisymmetric (i.e. $\partial\mathbf{u}/\partial\phi = 0$), (2.6)–(2.9) reduce to

$$-2v+P_r = -|\epsilon|(uu_r+d^{-1}wu_z-r^{-1}v^2)+E(u_{rr}+r^{-1}u_r-r^{-2}u+d^{-2}u_{zz}), \quad (2.11)$$

$$2u = -|\epsilon|(uv_r+r^{-1}uv+d^{-1}wv_z)+E(v_{rr}+r^{-1}v_r-r^{-2}v+d^{-2}v_{zz}), \quad (2.12)$$

$$d^{-1}P_z = -|\epsilon|(uw_r+d^{-1}ww_z)+E(w_{rr}+r^{-1}w_r+d^{-2}w_{zz}) \quad (2.13)$$

and

$$u_r+r^{-1}u+d^{-1}w_z = 0. \quad (2.14)$$

Distinguish solutions of the foregoing equations for the regions i, j, k, l and m by corresponding subscripts. In regions i and j (see figure 2), where all (dimensionless) length scales are of order unity, to zeroth order in $|\epsilon|$ and E, equations (2.11) to (2.14) satisfy the conditions under which equation (2.10) holds. For region i,

$$u_i = v_i = 0, \quad w_i = \mp E^{\frac{1}{2}} \operatorname{sgn} \epsilon, \quad P_i = 0, \tag{2.15}$$

which join smoothly with the Ekman boundary-layer solutions for regions k and l (see (2.19) and (2.20) below), where the upper sign applies to that part of region i lying above the disk, and the lower sign to the part below the disk. For region j,

$$u_j = 0, \quad v_j = -\tfrac{1}{2}r, \quad w_j = 0, \quad P_j = -\tfrac{1}{2}(r^2 - 1); \tag{2.16}$$

as this solution corresponds to the occurrence of no relative motion between region j and the container, there are no ageostrophic boundary layers where region j meets the end walls and side walls of the container.

Regions k and l are divergent Ekman boundary layers of thickness δ, where

$$\delta \equiv (\nu/\Omega)^{\frac{1}{2}} = aE^{\frac{1}{2}} \tag{2.17}$$

(see (1.3)), which satisfy the equations

$$\begin{aligned} -2v &= Ed^{-2}u_{zz}, \quad 2u = Ed^{-2}v_{zz}, \\ Ed^{-2}w_{zz} &= 0, \quad u_r + r^{-1}u + d^{-1}w_z = 0, \end{aligned} \tag{2.18}$$

obtained by setting $|\epsilon|$ equal to zero in equations (2.11) to (2.14), thus eliminating the non-linear inertial terms, and ignoring derivatives with respect to r in the viscous terms in the same equations, a valid procedure when $E \ll 1$ (see equation (2.17)). Solutions to these equations are as follows:

$$\begin{aligned} u_k &= \tfrac{1}{2}re^{-\sigma}\sin\sigma, \quad v_k = \tfrac{1}{2}re^{-\sigma}\cos\sigma, \\ w_k &= E^{\frac{1}{2}}\operatorname{sgn}\epsilon(1 - e^{-\sigma}(\cos\sigma + \sin\sigma)), \quad P_k = 0 = P_i, \end{aligned} \tag{2.19}$$

and

$$\begin{aligned} u_l &= -\tfrac{1}{2}re^{-\sigma}\sin\sigma, \quad v_l = -\tfrac{1}{2}re^{-\sigma}\cos\sigma, \\ w_l &= E^{\frac{1}{2}}\operatorname{sgn}\epsilon(1 - e^{-\sigma}(\cos\sigma + \sin\sigma)), \quad P_l = 0 = P_i, \end{aligned} \tag{2.20}$$

where $\sigma\delta$ is the perpendicular distance from the neighbouring rigid surface, $z' = -d'$ or $z' = (D' - d')$ for region l, and $z' = 0$ or $z' = b'$ for region k.

Observe that non-linear terms omitted in writing down (2.18) are of order $|\epsilon|$ or less times the included terms and are negligible, therefore, in the present approximation; this may be shown by substituting (2.19) or (2.20) into (2.11) to (2.13).

According to (2.15) and (2.16), across region m the azimuthal velocity v changes from its value $v_i = 0$ in region i to $v_j(r = 1) = -\frac{1}{2}$ at the edge of region j. Fluid enters and leaves region m where that region joins the Ekman layers, regions k and l. By continuity, w_m and w_i must on average have opposite signs (see (2.15)) and must be such that the total return flux in region m is equal to the net radial flux in the Ekman layers at $r = 1$, namely $\pi E^{\frac{1}{2}}$.

In region m, the detached shear layer, except near the 'corner' regions where region m meets regions k and l, the dominant derivatives are those with respect to r. The equations obtained by ignoring derivatives with respect to z in the

inertial and viscous terms of (2.11) and (2.14), and ignoring terms like u/r as small compared to terms like u_r, are:

$$\left.\begin{aligned} -2v+P_r &= -|\epsilon|uu_r+Eu_{rr}, \\ 2u &= -|\epsilon|uv_r+Ev_{rr}, \\ d^{-1}P_z &= -|\epsilon|uw_r+Ew_{rr}, \\ u_r+d^{-1}w_z &= 0. \end{aligned}\right\} \tag{2.21}$$

Although the experimental conditions were such that in most circumstances the terms involving $|\epsilon|$ were not small compared to those involving E, it is instructive to consider the case of negligible $|\epsilon|$. Equations (2.21) then reduce to

$$\left.\begin{aligned} -2v+P_r = Eu_{rr}, \quad 2u = Ev_{rr}, \\ P_z = dEw_{rr}, \quad u_r+d^{-1}w_z = 0, \end{aligned}\right\} \tag{2.22}$$

which are linear. Until a solution to (2.22) has been obtained under the appropriate boundary conditions, which will involve the discussion of the dynamics of the corner regions near the junctions of the detached shear layer with the Ekman layers, and of the flow generated at the vertical faces of the disk, the error arising in (2.21) from the neglect of non-linear terms cannot readily be ascertained. Crude arguments, based on nothing more than inspection of terms in (2.21) and (2.22), suggest that the neglect of non-linear terms might be justified when $|\epsilon|E^{-\frac{1}{4}}d^{-\frac{1}{2}}$ is small; the range of this quantity was 0·1 to 5, approximately, in the experiments described below.

Elimination of all but one of the variables (u) in (2.22) leads to the differential equation

$$E^2(u_{zz}+d^2u_{rr})_{rrrr}+4u_{zz} = 0. \tag{2.23}$$

This equation was obtained by Proudman (1956) in his analysis of flow between concentric spheres. Proudman's work stimulated a laboratory study by Fultz & Moore (to be published) and also led to a theoretical study of a geometrically simpler system in which Stewartson (1957) was able to obtain solutions to the equation.

Dimensionless length scales in the radial direction characteristic of the solutions of (2.23) are of order $E^{\frac{1}{3}}$ and $E^{\frac{1}{4}}$, and greater, therefore than the Ekman layer thickness, of order $E^{\frac{1}{2}}$. The existence of more than one length scale is an indication of the complexity of the structure of these boundary layers. Stewartson's work suggests that while the $E^{\frac{1}{3}}$ layer would be associated with the transport of fluid between region k and region l, it is across the $E^{\frac{1}{4}}$ layer that most of the change in v, from its value in region i to that in region j, takes place. Although the experiments described below give some indication of the gross features of the detached shear layers, owing to their small thickness no attempt was made to examine their detailed structure.

Topologically the flow we have just described is the same as that expected when $|\epsilon|$ is not much less than unity, as exemplified by the case $\Omega_0 = 0$, corresponding to $|\epsilon| = 2$. Viscous forces set the fluid in the vicinity of the disk into rotation and when $|\epsilon| = 2$ concomitant centripetal forces throw this fluid outwards well beyond the edge of the disk, thus inducing a general meridional circulation, with components towards the disk up to a certain distance from the axis of symmetry of the system, and away from the disk elsewhere.

When $|\epsilon| \ll 1$, although the flow is induced by viscous forces in ageostrophic regions on the bounding surfaces of the system, geostrophic flow must occur nearly everywhere else. Because geostrophic flow must be independent of z (see (2.10)), it is impossible for the meridional flow to penetrate into region j (see figure 2), which must, therefore, remain stagnant relative to the container (see (2.16)). Regions i, by rotating uniformly at a speed half-way between that of the disk and that of the container, are able to transport the axial flux required to match the radial flux in the Ekman layers (see (2.15)) without violating the Proudman–Taylor theorem, including the requirement that $\partial w/\partial z = 0$. By continuity there must be return flows connecting regions k to regions l outside regions i, and as these flows cannot occur in the geostrophic region j, they must occur in region m, the detached shear layer, whose thickness is sufficiently small to render the flow there highly ageostrophic.

3. Apparatus and techniques

The main apparatus consisted of a transparent cylindrical perspex (plexiglass) tank of uniform depth $D' = 30{\cdot}0$ cm and internal radius $R' = 19{\cdot}0$ cm (see figures 1 and 3). The perspex base and lid of the tank were bolted to flanges cemented around the top and bottom of the cylinder. Neoprene vacuum seals were incorporated in these cemented joints to keep them watertight. The side walls of the tank were 0·95 cm thick and the base and lid were 1·25 cm thick.

The tank rested with its axis vertical on three rollers, whose axes were horizontal and which were equally spaced around a central hole, 35 cm in diameter, in a horizontal plate of mild steel. The mild steel plate, which carried levelling screws, was mounted on a rigid cross-braced framework.

The tank was rotated at uniform angular velocity Ω_0 rad/s about its vertical axis by three further equally spaced rollers mounted on the mild-steel plate with their axes vertical. The rims of these rollers were in contact with the rim of the base of the tank. The rollers were connected together by a tightly stretched round belt (a vacuum seal ring) and one of them was coupled to a continuously variable drive consisting of a one-half horsepower electric motor and a variable-speed hydraulic transmission unit. The range of Ω_0 attainable in this way was 1 to 14 rad/s (see table 1).

The disk of radius a and thickness b' was also made of perspex. Five such disks, each of thickness $b' = 1{\cdot}25$ cm, were used in the present experiments (see, however, §8 below), the range of a thus obtained being 2·5–7·5 cm (see table 1). The disk was mounted on a hollow axle of outside diameter 1·27 cm, which passed through a flanged bush on the lid of the tank. After the apparatus had been assembled, this bush was aligned as follows. The centre of rotation of the lid was found by scribing a small circle on its upper face as it turned. A hole slightly larger than the diameter of the bush was then drilled at the centre of this circle. The bush was then bolted to the lid by round-headed screws passing through holes in the bush which were about 0·025 cm larger in diameter than the bolts themselves. Thus it was possible to align the axis of rotation of the disk with an accuracy of 0·002 cm.

The disk was rotated at Ω_1 rad/s by a separate continuously variable speed drive. The lowest reliable value of $|\epsilon|$ that could be obtained was 5×10^{-3} (see table 1). ϵ could be measured (by means of a stop-watch) to an accuracy of 0·5 %, and maintained constant with an accuracy of 1 % for periods of hours and longer.

The value of d', the distance from the tank base to the lower face of the disk, was always 22·0 cm.

The flow visualization technique employed most extensively in the experiments involved the introduction of neutrally buoyant dye (aqueous solution of crystal violet) into the space immediately below the disk via six holes of 0·04 cm diameter, each of which was connected to the hollow supporting axle of the disk by a channel in the disk. Small quantities of dye were introduced slowly, a drop at a time, into the hollow axle, until coloration appeared under the disk.

Visual and photographic observations were facilitated by the use of a rotoscope, consisting of a Dove prism whose optical axis coincided with the axis of rotation of the tank and which rotated about that axis with angular velocity $\frac{1}{2}\Omega_1$ rad/s. Apart from the effects of slight optical aberrations of the prism, the image of the disk as viewed through the rotoscope was stationary.

Axial fluid motions in regions i and m (see figure 2) were determined by timing the movement of dye over distances measured by means of a cathetometer.

4. Régimes of flow

In this section we shall consider qualitative aspects of the axisymmetric and non-axisymmetric régimes of flow (see (1.5)) for the two cases $\epsilon > 0$ and $\epsilon < 0$.

Axisymmetric régime, ϵ positive

Observations confirm that the axisymmetric régime has the general properties predicted by the theoretical discussion in §2 above. Regions i rotate at a uniform speed intermediate between that of the tank and that of the disk, and region j rotates with the tank (see (2.15) and (2.16)). Across regions k and l (Ekman layers of thickness δ (see (2.17)) never more than 0·1 cm) the azimuthal motion varies rapidly, from its uniform value in region i to that of the disk in the case of regions k and to that of the tank in the case of regions l (see (2.19) and (2.20)). Across region m, the detached shear layer the thickness of which was usually several millimetres, the azimuthal motion varies from that of regions i to that of region j (see (2.15) and (2.16)).

Superimposed on this azimuthal field of flow is a meridional field (see figure 3, plate 1). Accordingly, fluid particles spiral outwards in regions k and inwards in regions l (see (2.19) and (2.20)). Continuity demands that particles should move axially towards the disk from regions l to regions i, and in the opposite directions in region m (see figure 2). w_i, the rate of axial drift in regions i, is independent of r and z (see (2.15)). Its value is given by the 'Ekman suction' formula for a divergent Ekman layer, which relates the magnitude of the flow out of the Ekman layer to the vorticity of the interior flow (see Prandtl 1953).

As the thickness of region m is smaller than the radius of the disk, the average

speed of the return flow in that region is much greater than w_i. Unlike w_i, w_m varies rapidly with r and z and in a complicated way, involving axial motions in both directions.

Motions in the 'corner' regions, where the detached shear layer meets the Ekman layers, were complicated and have not yet been studied in detail. There was no evidence in the experiment that flow occurred from one side of the disk to the other.

Axisymmetric régime, ϵ negative

When the disk rotates more slowly than the tank, ϵ is negative. The main effect of altering the sign of ϵ is the reversal of the direction of the relative flow. Certain details of the structure of the corner regions seem, however, to depend on the sign of ϵ.

Non-axisymmetric régime, ϵ positive

When $|\epsilon| > |\epsilon_T|$, (see (1.5)), the axisymmetric flow gives way to non-axisymmetric flow. In a typical experiment with ϵ positive, if ϵ is increased gradually from zero, axisymmetric flow occurs until ϵ reaches the value ϵ_T. At this point region m becomes misshapen. When viewed along the axis of rotation the generators of the sides of region m form not a circle, but an oval, triangle, square or a pentagon, etc. (see figure 4), depending, as we shall see in §7 below, on E (see (1.3)). Wave-like protuberances showing little or no dependence on z extend from the polygonal region m into what had been, in the axisymmetric régime, region j. The general features of the meridional circulation do not change significantly when the waves make their appearance.

Increasing ϵ still further brings about changes in the wave-number, M; the dependence of M on ϵ is discussed in §7 below.

Non-axisymmetric régime, ϵ negative

When ϵ is negative, although axisymmetric flow gives way to non-axisymmetric flow when ϵ exceeds a certain critical value, the pattern of flow is quite different from that occurring when ϵ is positive. Instead of undergoing a wave-like distortion that penetrates into region j, region m distorts into an off-axis ellipse (as viewed along the axis of rotation) that disturbs the flow in regions i as well as in region j (see figure 5). Figure 5, which is an attempt to illustrate this distortion, should be regarded as schematic, since the addition of dye tended to obscure the finer features of the flow. Although the onset of non-axisymmetric flow was easy to observe, it was difficult to photograph well.

5. Transition between axisymmetric and non-axisymmetric flow

The results of an investigation of the dependence of ϵ_T, the value of ϵ at the transition between axisymmetric and non-axisymmetric flow, on a and Ω are presented in table A 1. This table includes 25 determinations for $\epsilon > 0$ and three determinations for $\epsilon < 0$. Evidently even though the form of the non-axisymmetric flow depends strongly on the sign of ϵ (see figures 4 and 5, plate 2), the

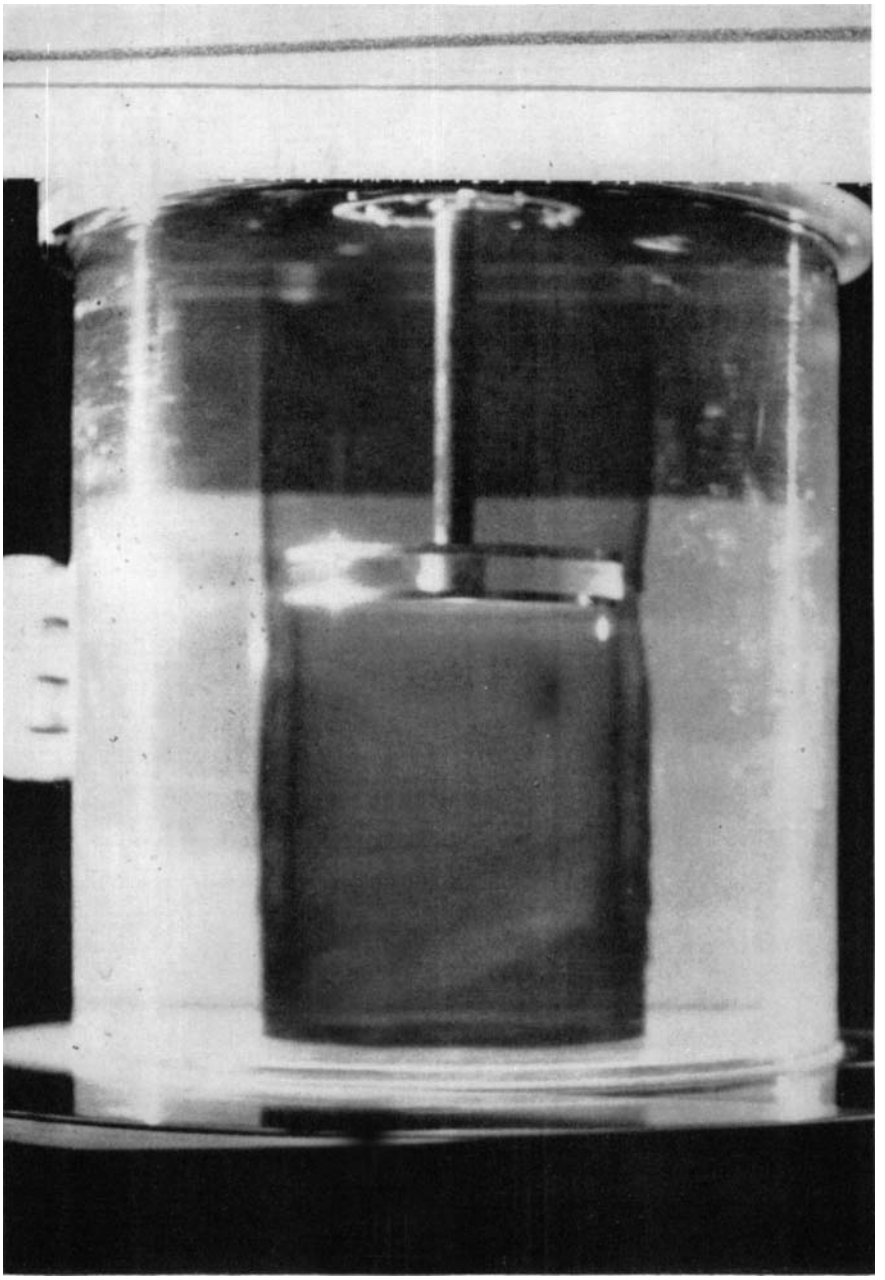

FIGURE 3. Illustration of the axisymmetric régime of flow. The photograph was taken after a sufficient lapse of time following the commencement of the continuous release of dye from the rim of the disk for the dye to have completed more than one meridional 'circuit'. (The axle of the rotating disk can be seen in the upper part of the picture.)

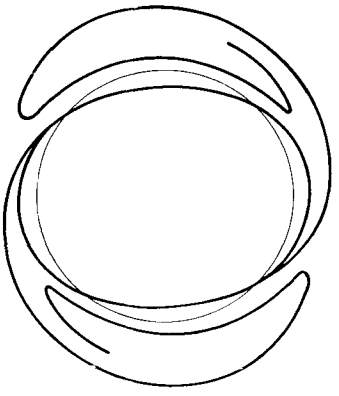

FIGURE 4(*a*)

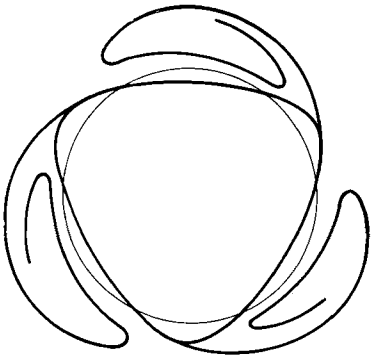

FIGURE 4(*b*)

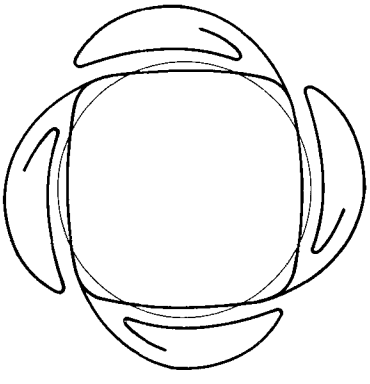

FIGURE 4(*c*)

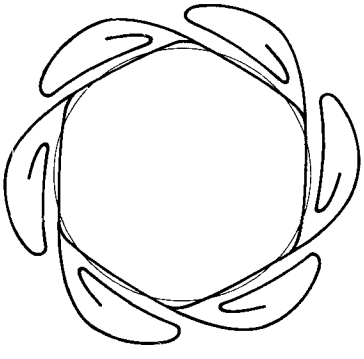

FIGURE 4(*d*)

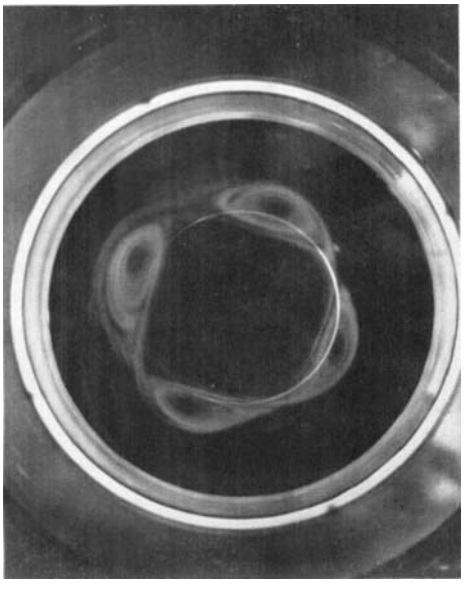

FIGURE 4(*e*)

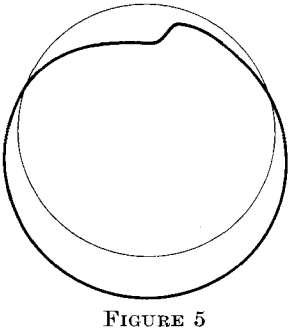

FIGURE 5

FIGURE 4. Illustration of the forms taken by the non-axisymmetric detached shear layer when $\epsilon > 0$ (cf. figure 5). For experimental details see figure 9. (*a*), (*b*), (*c*) and (*d*) are sketches based on visual studies. (*e*) is a photograph obtained in a new series of experiments, the results of which are not yet published, obtained by suspending aluminium powder in the fluid and illuminating the system with a flat beam of light.

FIGURE 5. Illustration of the form taken by the non-axisymmetric detached shear layer when $\epsilon < 0$ (cf. figure 4). Experimental details: $a = 5{\cdot}00$ cm, $E^{-1} = 26{\cdot}3 \times 10^3$, $\epsilon = -0{\cdot}055$.

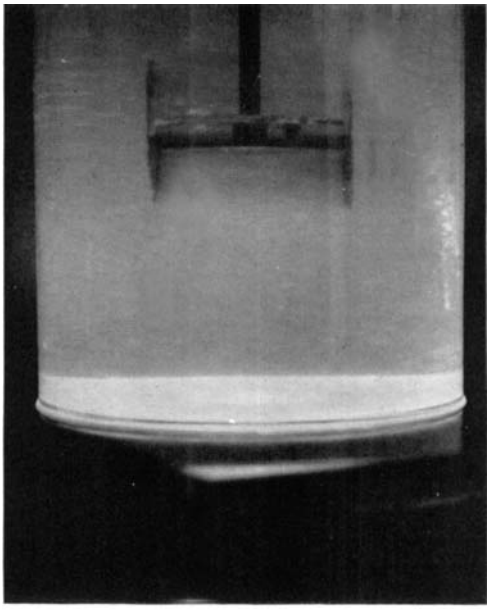

(*a*)

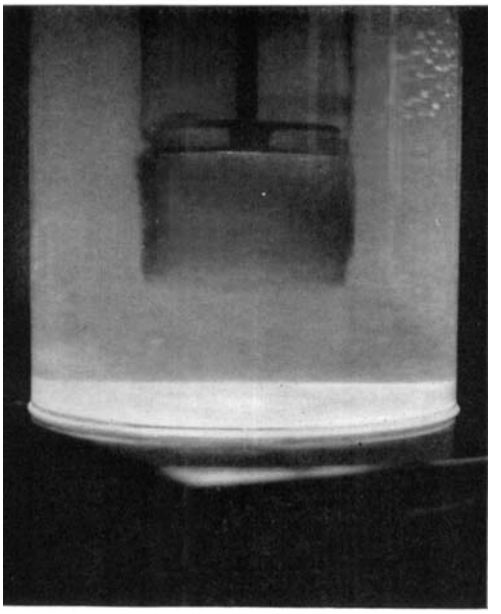

(*b*)

FIGURE 7. Illustration of the motion in region m (see figure 2). Photograph (*a*) was taken 4 min after the commencement of the continuous release of dye from the rim of the disk and (*b*) was taken 4 min after (*a*). Experimental details: $\Omega_0 = 5{\cdot}30$ rad/s, $\Omega_1 = 5{\cdot}45$ rad/s, corresponding to $\epsilon = 0{\cdot}028$.

value of $|\epsilon_T|$ does not. Values of the wave-number, M, of the flow occurring at the transition are also given in table A 1.

The results of table A 1 are plotted in figure 6, which indicates clearly that there is a good straight-line relationship between $\log|\epsilon_T|$ and $\log E$. The equation of the

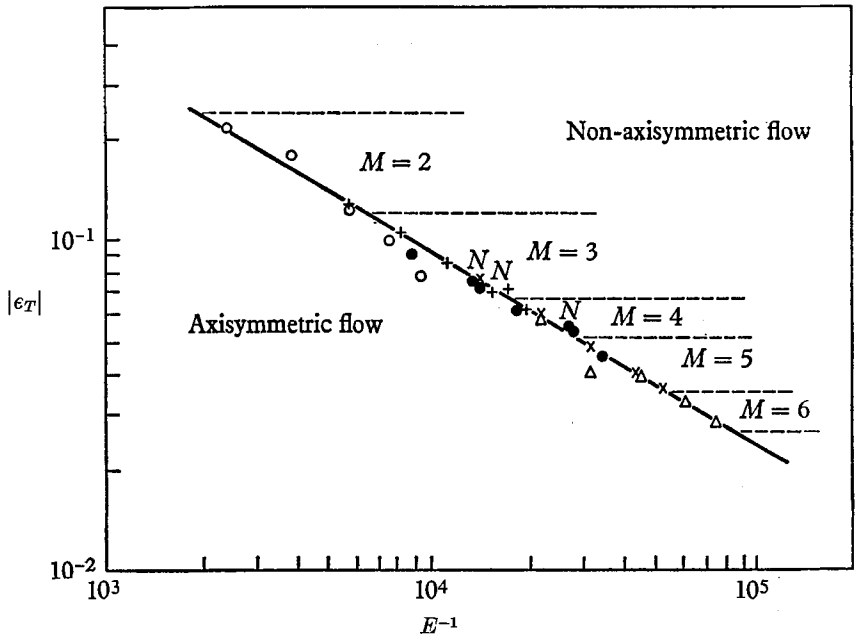

FIGURE 6. The régime transition results for $\epsilon > 0$ and $\epsilon < 0$. The symbols have the following meanings:

symbol	○	+	●	×	△
a (cm)	2·5	3·75	5·00	6·25	7·50

The points for which $\epsilon < 0$ are indicated by a letter N. The broken lines indicate regions of different wave number M at the transition when $\epsilon > 0$ (cf. figures 4, 5 and 9). (For details see table A 1.) The best straight line through all the 25 points for $\epsilon > 0$ is

$$\log_{10}|\epsilon_T| = 1{\cdot}225 \pm 0{\cdot}055 - (0{\cdot}586 \pm 0{\cdot}013)\log_{10}E^{-1} \text{ (standard errors).}$$

best straight line through the points for $\epsilon > 0$ is given by (1.5). The discussion of the physical significance of the coefficients A and n will be deferred to another paper describing experiments still in progress on the dependence of ϵ_T on the further parameters ν, b' and d'. It may, however, be significant that $n = 0{\cdot}568 \pm 0{\cdot}013$ is close to four-sevenths (0·5714)!

6. The axisymmetric régime

According to (2.15), below the disk

$$w_i' = \nu^{\frac{1}{2}}\Omega^{\frac{1}{2}}\epsilon \tag{6.1}$$

to zeroth order in ϵ. On releasing dye from the lower rim of the disk when $\epsilon < 0$ it was found that the Ekman layer flow on the disk quickly carried the dye towards the axis. This was followed by a slow descent of dye at a rate showing no

dependence on r, in agreement with the last equation. Using water at 20·2 °C, so that $\nu = 1{\cdot}01 \times 10^{-2}\,\mathrm{cm^2 s^{-1}}$, and $\Omega_0 = 10{\cdot}85\,\mathrm{rad/s}$, $a = 5{\cdot}0\,\mathrm{cm}$, and two values of ϵ, namely $-0{\cdot}0126$ and $-0{\cdot}0255$, the following results were obtained:

Distance below disk (cm)	Time in minutes at which dye first reached level given in left column (zero of time arbitrary)	
	$\epsilon = -0{\cdot}126$	$\epsilon = -0{\cdot}0255$
0·85	5·0	—
2·0	10·5	5·0
4·0	21·2	11·5
6·0	32·5	18·5
8·0	43·5	—
10·0	55·0	—

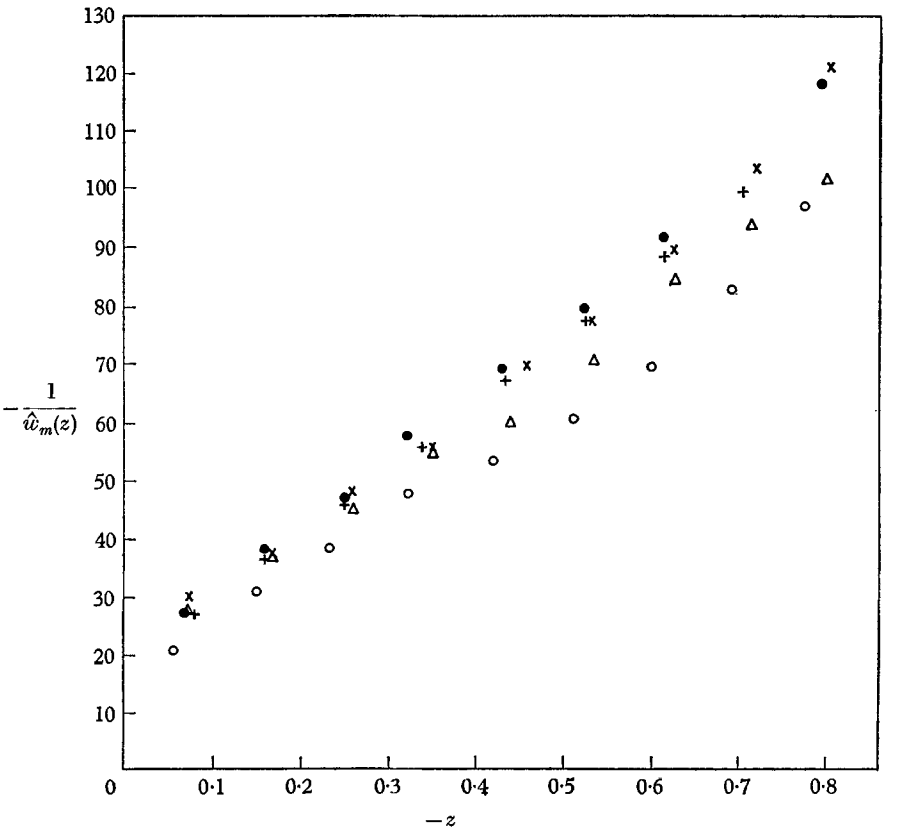

FIGURE 8. Illustration of typical variation of $1/\hat{w}_m(z)$ with z, suggesting that $\hat{w}_m = \tilde{w}_m/(1+z/Z_m)$, where $\tilde{w}_m$ and Z_m depend on E. Tables A 2 give complete results for $\hat{w}_m$ versus z and table 2 lists the corresponding values of $\tilde{w}_m^{-1}$ and Z_m. Experimental details:

FIGURE 8 (a): $\Omega_0 = 10{\cdot}85\,\mathrm{rad/s}$, $d' = 22{\cdot}01\,\mathrm{cm}$:

symbol	○	+	●	×	△
a (cm)	2·50	3·75	5·00	6·25	7·50

These measurements suggest that $w_i' = 0{\cdot}184\epsilon$, which is in good agreement with the theoretical value based on (6.1), namely $w_i' = 0{\cdot}175\epsilon$. They also suggest that the axial velocity at which the dye, owing to its very slight negative buoyancy, moved relative to the fluid was $-0{\cdot}69 \times 10^{-3}$ cm/s. The buoyancy correction is significant here because the axial motions in the interior region were incredibly slow. (Owing to the relatively rapid axis flow in the detached shear layers buoyancy effects were quite negligible there (see figure 2).) The few measurements that were made of the dependence of v on r at a level below the disk well above region l and below region k were consistent with (2.15) and (2.16) and indicated that the thickness of the region m is a good deal greater than δ (see (2.17)) in accordance with the discussion following (2.23)).

Figure 7, plate 3 illustrates the axial motion in region m when $\epsilon > 0$. The first photograph (see figure 7*a*) was taken 4 min after the commencement of the continuous release of dye from the rim of the disk, and the second photograph

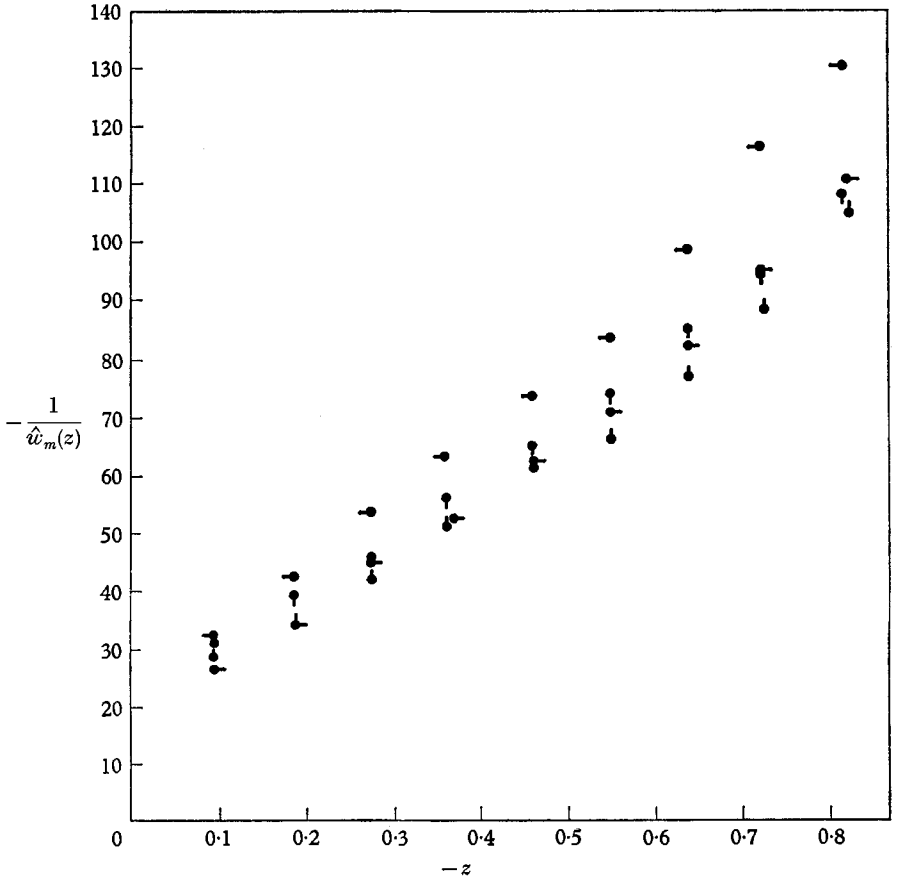

FIGURE 8(*b*): $a = 5{\cdot}00$ cm, $d' = 22{\cdot}01$ cm:

symbol	●	●	●	●
Ω_0(rad/s)	4·18	6·28	8·37	13·61

(figure 7*b*) was taken 4 min later. The instantaneous rate of advance of the edge of the ink cylinder is a measure of $\hat{w}'_m$ (see (1.6)), the value of w'_m at the extremum of the profile of w'_m across the detached shear layer. A systematic investigation of this quantity, whose dimensionless value we denote by $\hat{w}_m$ (see (1.6) and (2.4)), was undertaken. The results are listed in table A 2 and plotted in figure 8.

Inspection of figure 8 suggests that there is a fairly good straight-line relationship between $\hat{w}_m^{-1}$ and z, in which case these quantities are related by the expression

$$\hat{w}_m(z) = \tilde{w}_m/[1 + z/Z_m] \tag{6.2}$$

(the dimensionless form of (1.6)). The values of $\tilde{w}_m^{-1}$ and Z_m corresponding to the best fit of the experimental data to the last expression are given in table 2. The variation of $\tilde{w}_m$ and Z_m is remarkably slight over the range of ϵ, E and d covered.

a (cm)	Ω_0 (rad/s)	$E \times 10^5$	$\epsilon \times 10^2$	$d^{-1} \times 10$	$(-\tilde{w}_m)^{-1}$	$-Z_m$
2·50	10·85	14·1–14·6	3·41–9·97	1·14	14·1	0·142
3·75	10·85	6·43–6·60	2·27–6·48	1·70	16·9	0·142
5·00	4·18	9·42	6·88	2·27	15·0	0·147
5·00	6·28	6·27	5·04	2·27	13·1	0·116
5·00	8·37	4·73	3·66	2·27	19·2	0·185
5·00	10·85	3·63–3·70	1·47–5·62	2·27	16·6	0·133
5·00	13·61	2·71	3·92	2·27	18·3	0·143
6·25	10·85	2·34–2·36	1·69–3·57	2·84	18·7	0·161
7·50	10·85	1·64–1·65	1·69–2·35	3·41	18·9	0·187

TABLE 2. Values of $\tilde{w}_m^{-1}$ and Z_m corresponding to the best fit of the expression $\hat{w}_m(z) = \tilde{w}_m/(1 + z/Z_m)$ to the data of figure 8 (see also table A 2)

7. The non-axisymmetric régime

As the elucidation of the detailed properties of the non-asymmetric flow described in §§4 and 5 above lies beyond the scope of the present paper and will have to be reported elsewhere, we shall restrict attention here to the case of positive ϵ, and consider two properties only of the waves that then occur, namely, their wave-number, M, and their uniform rate of drift, $(\Omega_w - \Omega)$ rad/s, relative to a frame of reference which rotates at Ω rad/s with respect to the laboratory (see equation (2.1)).

Table A 3 gives all the determinations of M with the exception of those found at the transition between axisymmetric and non-axisymmetric flow, together with the values of ϵ and E at which they were made. According to figure 9, which displays these results in a ϵ versus E^{-1} diagram, M is a decreasing function of ϵ and does not depend strongly on E. The presence of transitional regions in which more than one wave-number occurred (see figure 9) is probably due to hystersis effects, associated with the manner in which a point in parameter space is approached, and with 'vacillations' in the flow pattern which manifest themselves as regular fluctuations in the properties of the waves (see Hide 1953, 1966).

Figure 10 gives all the determinations of Ω_w as expressed by the parameter

$$\epsilon_w \equiv (\Omega_w - \Omega)/\Omega \tag{7.1}$$

(see (2.1), cf. (1.2)), made with the apparatus described in § 3 above (see also table 1), plus a few additional determinations at relatively high values of ϵ made with another piece of apparatus of somewhat different dimensions (see legend to figure 10). It is interesting that ϵ_w is negative, always greater than $-0{\cdot}5\epsilon$, and varies smoothly with ϵ slightly faster than linearly. Had the waves been stationary relative to the tank, ϵ_w would be equal to $-0{\cdot}5\epsilon$; had the waves been stationary relative to the disk, ϵ_w would be equal to $0{\cdot}5\epsilon$.

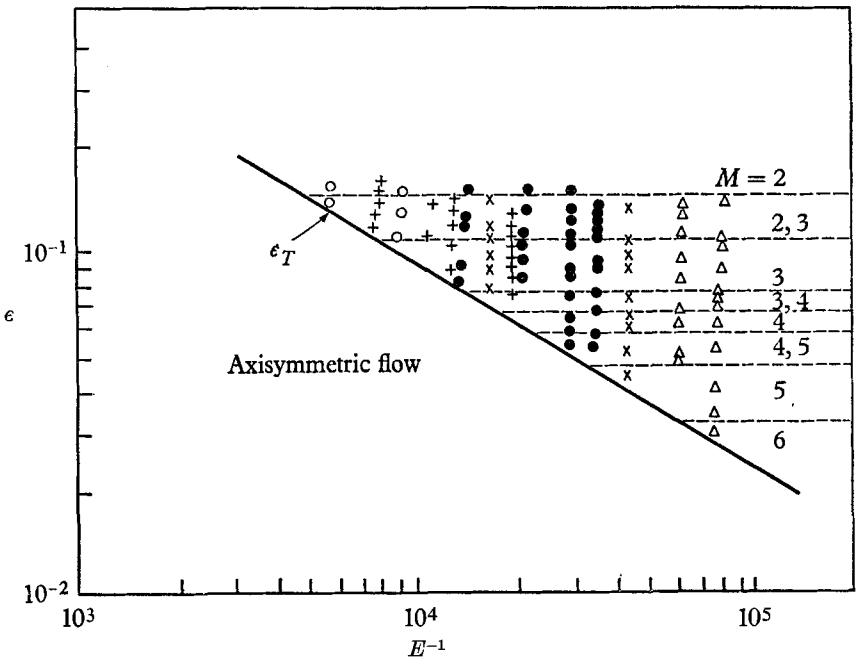

FIGURE 9. All the wave-number determinations, excluding those given in figure 4 (see table A 3), displayed in an ϵ versus E^{-1} diagram. The symbols have the following meanings:

symbol	○	+	●	×	△
a (cm)	2·50	3·75	5·00	6·25	7·50

The full line separates the axisymmetric flow régime from the wave régime (see figure 4). The broken lines divide the wave régime according to the observed wave-numbers.

8. Concluding remarks

Although the foregoing experiments (*a*) verify the theoretical prediction that detached shear layers should occur when $|\epsilon|$ and E are much less than unity, (*b*) show that the axisymmetric flow gives way to non-axisymmetric flow under quite definite and reproducible conditions, and (*c*) elucidate certain additional properties of the non-axisymmetric flow, they leave a number of questions unanswered and raise certain new questions. These questions are now being investigated in a series of new experiments in which both complications and simplifications in the

apparatus are introduced. Of particular interest, for example, are the detailed structure of the detached shear layer and the dependence of A and n on ν, b', d', etc. (see (1.5) and figure 1). When these new experiments have been completed it will be possible to formulate some of the theoretical problems raised by the investigation, the most interesting of which being, presumably, that of accounting for the occurrence of non-axisymmetric flow.

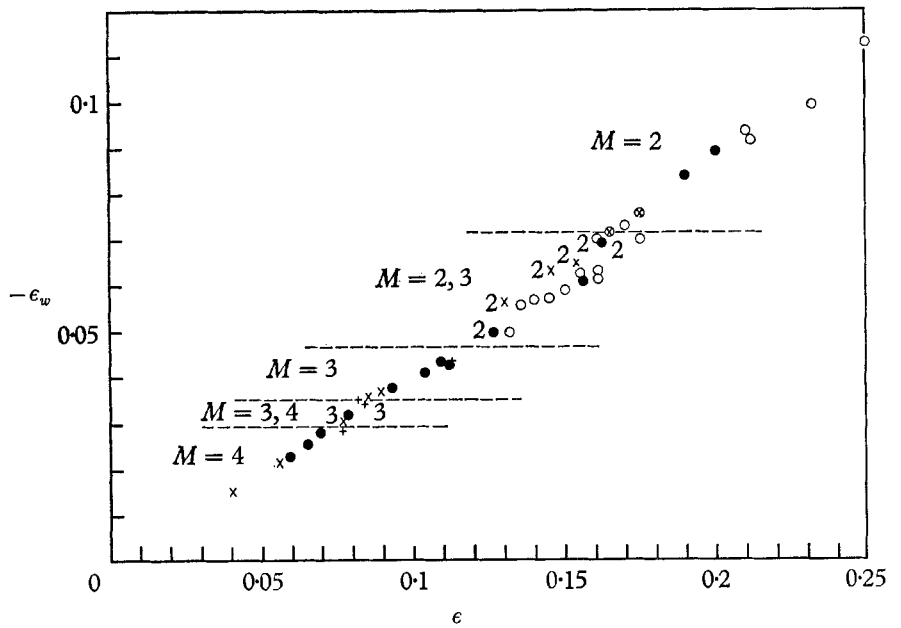

FIGURE 10. All the determinations of $(\Omega_w - \Omega)$, the drift angular velocity of the waves in a frame rotating at $\Omega \equiv \frac{1}{2}(\Omega_0 + \Omega_1)$ rad/s relative to a co-ordinate frame fixed in the laboratory, expressed in terms of $\epsilon_w \equiv (\Omega_w - \Omega)/\Omega$ and plotted against $\epsilon \equiv (\Omega_1 - \Omega_0)/\Omega$. The symbols have the following meanings:

symbol	○	+	●	×	△
a (cm)	2·50	3·75	5·00	6·25	7·50

The results for $a = 2{\cdot}50$ cm were obtained with a demonstration apparatus for which $b' = 1{\cdot}23$ cm, $d' = 10{\cdot}9$ cm, $D' = 31{\cdot}3$ cm, $R' = 14{\cdot}5$ cm, and $\nu = 0{\cdot}0095$ cm^{2}s^{-1}; the other results were obtained under the conditions listed in table 1.

The research described in this paper, the principal results of which were first presented in full in 1961 and 1962 in reports prepared under contract AF-61(052)-216, Cambridge Research Laboratories, Office of Aerospace Research (European Office), United States Air Force, is part of a programme which has also received financial support through grants from the British Department of Scientific and Industrial Research and the Royal Society of London to King's College (University of Durham), Newcastle upon Tyne (now the University of Newcastle upon Tyne), and from the National Science Foundation (Atmospheric Sciences Programme) to the Massachusetts Institute of Technology.

Appendix

The following tables contain, respectively, all the ϵ_T determinations presented graphically in figure 6, together with values of the wave-number, M, occurring at the transition from axisymmetric to non-axisymmetric flow (table A 1), all the $\hat{w}_m(z)$ determinations upon which figures 8 are based (table A 2), and all the determinations of M excluding those given in table A 1, upon which figure 9 is based (table A 3).

a (cm)	$E^{-1} \times 10^{-3}$	ϵ_T	M
2·50	2·24	0·218	2
	3·58	0·184	2
	5·20	0·125	2
	7·11	0·104	3
	8·46	0·082	3
3·75	5·17	0·127	2
	7·70	0·109	3
	11·30	0·083	3
	14·6	−0·073	–
	15·7	0·074	3
	18·8	0·063	4
5·00	8·37	0·095	3
	12·6	−0·078	–
	13·4	0·073	3
	17·6	0·063	4
	26·3	−0·055	–
	27·7	0·053	4
	34·0	0·045	5
6·25	13·5	0·077	3
	21·2	0·059	4
	31·4	0·046	5
	43·0	0·039	5
	51·6	0·035	5
7·50	21·7	0·058	4
	30·2	0·038	5
	44·5	0·039	5
	61·7	0·032	6
	74·5	0·028	6

TABLE A 1. All the ϵ_T determinations (see figure 6). Values of the wave number, M, at the transition are given in the third column (see figure 4). When $\epsilon < 0$ the non-axisymmetric flow has the form illustrated by figure 5.

(*a*) $a = 2{\cdot}50$ cm, $\Omega_0 = 10{\cdot}85$ rad/s ($E \times 10^5 = 14{\cdot}1$–$14{\cdot}6$, $d^{-1} = 0{\cdot}114$)

	$-\hat{w}_m(z) \times 10^2$			
$-z$	$\epsilon = 0{\cdot}0341$	$\epsilon = 0{\cdot}0578$	$\epsilon = 0{\cdot}0722$	$\epsilon = 0{\cdot}0997$
0·057	4·80	4·72	4·86	4·93
0·147	3·20	2·92	3·41	3·22
0·238	2·52	2·64	2·57	2·64
0·328	2·04	2·23	2·09	2·12
0·419	1·84	1·96	1·82	1·85
0·510	1·69	1·73	1·54	1·65
0·601	1·46	1·48	1·31	1·41
0·691	1·31	1·22	1·08	1·16
0·782	1·10	1·02	0·93	1·02
0·872	0·99	0·82	0·75	0·85

(*b*) $a = 3{\cdot}75$ cm, $\Omega_0 = 10{\cdot}85$ rad/s ($E \times 10^5 = 6{\cdot}43$–$6{\cdot}60$, $d^{-1} = 0{\cdot}170$)

	$-\hat{w}_m(z) \times 10^2$				
$-z$	$\epsilon = 0{\cdot}0227$	$\epsilon = 0{\cdot}0321$	$\epsilon = 0{\cdot}0381$	$\epsilon = 0{\cdot}0572$	$\epsilon = 0{\cdot}0648$
0·070	3·73	3·62	3·66	3·94	3·69
0·161	2·75	2·58	2·77	2·70	2·95
0·251	2·17	2·10	2·22	2·14	2·26
0·342	1·78	1·78	1·80	1·79	1·76
0·432	1·46	1·46	1·50	1·50	1·48
0·523	1·28	1·33	1·22	1·30	1·26
0·614	—	1·13	1·09	1·12	1·14
0·704	—	1·00	0·96	0·95	0·99
0·795	—	0·85	0·86	0·88	0·86

(*c*) $a = 5{\cdot}00$ cm, $\Omega_0 = 4{\cdot}18$ rad/s ($E \times 10^5 = 9{\cdot}42$, $\epsilon = 0{\cdot}0688$, $d^{-1} = 0{\cdot}227$)

$-z$	$-\hat{w}_m(z) \times 10^2$
0·094	3·56
0·184	2·89
0·275	2·59
0·366	1·95
0·457	1·64
0·548	1·40
0·638	1·30
0·729	1·13
0·820	0·95

(*d*) $a = 5{\cdot}00$ cm, $\Omega_0 = 6{\cdot}28$ rad/s ($E \times 10^5 = 6{\cdot}27$, $\epsilon = 0{\cdot}0504$, $d^{-1} = 0{\cdot}227$)

$-z$	$-\hat{w}_m(z) \times 10^2$
0·094	3·79
0·184	2·82
0·275	2·22
0·366	1·88
0·457	1·59
0·548	1·41
0·638	1·21
0·729	1·05
0·820	0·90

TABLE A 2. All the $\hat{w}_m(z)$ determinations (see figures 8 and table 2)

(*e*) $a = 5{\cdot}00$ cm, $\Omega_0 = 8{\cdot}37$ rad/s ($E \times 10^5 = 4{\cdot}73$, $\epsilon = 0{\cdot}0366$, $d^{-1} = 0{\cdot}227$)

$-z$	$-\hat{w}_m(z) \times 10^2$
0·094	3·19
0·184	2·56
0·275	2·16
0·366	1·76
0·457	1·52
0·548	1·25
0·638	1·16
0·729	1·07
0·820	0·93

(*f*) $a = 5{\cdot}00$ cm, $\Omega_0 = 10{\cdot}85$ rad/s ($E \times 10^5 = 3{\cdot}63$–$3{\cdot}70$, $d^{-1} = 0{\cdot}227$)

	$-\hat{w}_m(z) \times 10^2$					
$-z$	$\epsilon = 0{\cdot}0147$	$\epsilon = 0{\cdot}0218$	$\epsilon = 0{\cdot}0294$	$\epsilon = 0{\cdot}0372$	$\epsilon = 0{\cdot}0490$	$\epsilon = 0{\cdot}0562$
0·069	3·59	3·52	3·48	3·68	3·76	3·74
0·160	2·51	2·73	2·37	2·68	2·75	2·69
0·250	2·10	2·17	2·00	2·04	2·11	2·30
0·341	1·82	1·66	1·68	1·69	1·74	1·71
0·431	1·51	1·36	1·37	1·38	1·50	1·51
0·522	1·25	1·26	1·21	1·17	1·33	1·25
0·613	1·13	1·07	1·02	1·08	1·14	1·07
0·703	1·07	0·94	0·92	0·92	0·98	0·89
0·794	1·00	—	0·79	0·83	0·80	0·76
0·886	—	—	0·70	0·71	0·63	0·63

(*g*) $a = 5{\cdot}00$ cm, $\Omega_0 = 13{\cdot}61$ rad/s ($E \times 10^5 = 2{\cdot}71$, $\epsilon = 0{\cdot}0392$, $d^{-1} = 0{\cdot}227$)

$-z$	$-\hat{w}_m(z) \times 10^2$
0·094	3·10
0·184	2·31
0·275	1·85
0·366	1·57
0·457	1·34
0·548	1·18
0·638	1·00
0·729	0·85
0·820	0·74

(*h*) $a = 6{\cdot}25$ cm, $\Omega_0 = 10{\cdot}85$ rad/s ($E \times 10^5 = 2{\cdot}34$–$2{\cdot}36$, $d^{-1} = 0{\cdot}284$)

	$-\hat{w}_m(z) \times 10^2$				
$-z$	$\epsilon = 0{\cdot}0169$	$\epsilon = 0{\cdot}0214$	$\epsilon = 0{\cdot}0249$	$\epsilon = 0{\cdot}0317$	$\epsilon = 0{\cdot}0357$
0·080	3·30	3·17	3·34	3·32	3·24
0·170	2·65	2·69	2·46	2·73	2·61
0·260	2·29	1·95	1·99	2·22	2·07
0·351	1·94	1·86	1·72	1·73	1·59
0·441	1·51	1·40	1·34	—	1·43
0·532	1·23	1·19	1·22	1·37	1·32
0·623	1·18	1·06	1·12	1·11	1·09
0·713	1·08	0·92	0·91	0·93	0·97
0·804	—	—	0·79	0·79	0·86

TABLE A 2—*continued*

(*i*) $a = 7{\cdot}50$ cm, $\Omega_0 = 10{\cdot}85$ rad/s ($E \times 10^5 = 1{\cdot}64$–$1{\cdot}65$, $d^{-1} = 0{\cdot}341$)

	$-\hat{w}_m(z) \times 10^2$			
$-z$	$\epsilon = 0{\cdot}0169$	$\epsilon = 0{\cdot}0198$	$\epsilon = 0{\cdot}0227$	$\epsilon = 0{\cdot}0235$
0·080	3·45	3·61	3·45	3·87
0·170	2·59	2·64	2·82	2·88
0·260	2·20	2·21	2·19	2·27
0·351	1·84	1·77	1·74	1·94
0·441	1·57	—	1·65	1·72
0·532	1·39	1·36	1·39	1·50
0·623	1·25	1·24	1·23	1·29
0·713	1·01	1·07	1·03	1·12
0·804	—	—	—	0·98

TABLE A 2—*continued*

a (cm)	$E^{-1} \times 10^{-3}$	ϵ	M
2·50	5·55	0·139	2
	5·60	0·157	2
	8·58	0·113	3
	8·67	0·133	2
	8·76	0·150	2
3·75	7·86	0·111	3
	7·95	0·129	2, 3
	8·00	0·136	2, 3
	8·05	0·149	2
	8·10	0·161	2
	10·80	0·112	3
	10·82	0·115	3?
	10·83	0·117	2, 3
	10·95	0·137	2
	12·2	0·089	3
	12·3	0·098	3
	12·4	0·112	3
	12·5	0·128	2, 3
	12·6	0·142	2
	19·1	0·0735	3?
	19·2	0·083	3
	19·25	0·090	3
	19·35	0·0975	3
	19·4	0·102	3
	19·5	0·1125	3
	19·6	0·1205	2, 3
	19·7	0·129	2
5·00	13·5	0·0795	3
	13·6	0·0915	3
	13·8	0·121	3
	13·85	0·126	2, 3
	14·05	0·149	2
	20·5	0·084	3
	20·6	0·095	3
	20·7	0·102	3

TABLE A 3. All the determinations of M, the wave-number, excluding those given in table A 1 (see figure 9; cf. figure 4).

a (cm)	$E^{-1} \times 10^{-3}$	ϵ	M
5·00	20·8	0·104	3
	21·0	0·113	3
	21·1	0·118	2, 3
	21·2	0·129	2, 3
	21·3	0·138	2
	21·4	0·152	2
	27·1	0·053	4
	27·2	0·057	4
	27·25	0·0635	4
	27·4	0·0752	3
	27·5	0·0855	3
	27·6	0·0885	3
	27·8	0·102	3
	28·0	0·114	3
	28·1	0·125	2, 3
	28·3	0·138	2, 3
	28·5	0·148	2
	34·5	0·0503	5
	34·9	0·0593	4
	35·0	0·0675	3, 4
	35·0	0·068	3
	35·1	0·076	3
	35·5	0·094	3
	35·6	0·098	3
	35·8	0·112	3
	35·9	0·1175	2, 3
	36·1	0·1275	2, 3
	36·2	0·1315	2
	36·4	0·141	2
6·25	17·25	0·078	3
	17·35	0·088	3
	17·4	0·095	3
	17·55	0·1085	3
	17·7	0·129	3
	17·85	0·142	2
	43·1	0·0441	5
	43·8	0·0507	4
	44·0	0·061	4
	44·1	0·0669	3, 4
	44·3	0·0752	3
	44·5	0·0908	3
	44·8	0·0985	3
	45·1	0·1095	3
	45·2	0·116	3
	45·6	0·132	2
7·50	62·0	0·048	5
	62·1	0·0515	4, 5
	62·5	0·0625	4
	62·7	0·0677	4
	62·8	0·0695	3, 4
	63·3	0·0837	3
	63·7	0·0971	3
	64·4	0·122	2, 3
	64·6	0·1295	2,3
	64·9	0·136	2

TABLE A 3—*continued*

a (cm)	$E^{-1} \times 10^{-3}$	ϵ	M
7·50	76·6	0·0295	6
	77·0	0·0345	5
	77·1	0·0418	5
	77·5	0·0532	4
	78·0	0·0652	4
	78·1	0·0662	3, 4
	78·4	0·0707	3
	78·8	0·0775	3
	79·3	0·0905	3
	79·5	0·1035	3
	80·1	0·118	3
	81·2	0·1395	2

TABLE A3—*continued*

REFERENCES

HIDE, R. 1953 *Quart. J. Roy. Met. Soc.* **79**, 161.

HIDE, R. 1966 *Bull. Am. Met. Soc.* **47**, 873.

PRANDTL, L. 1952 *Essentials of Fluid Dynamics*. London: Blackie, 452 pp. (See especially pp. 356–364.)

PROUDMAN, I. 1956 *J. Fluid Mech.* **1**, 505.

PROUDMAN, J. 1916 *Proc. Roy. Soc. Lond.* A, **92**, 408.

STEWARTSON, K. 1957 *J. Fluid Mech.* **3**, 17.

TAYLOR, G. I. 1923 *Proc. Roy. Soc. Lond.* A, **104**, 213.